JMEPEG (2020) 29:3678–3687
https://doi.org/10.1007/s11665-020-04812-y

1059-9495/$19.00

Modification of Mg_2Si Phase Morphology in Mg-4Si Alloy by Sb and Nd Additions

Hao Dong, Siming Xiang, Jie Lv, Yu Wang, Lu Li, and Wenbin Yu

(Submitted December 4, 2019; Accepted: 14 April 2020; published online June 22, 2020)

We reported the effects of compound modification with Nd and Sb on the microstructure evolution and mechanical properties of Mg-4Si alloys. The characterization results showed that adding 1.0 wt.% Sb and 1.0 wt.% Nd to the alloy can effectively change the morphology of Mg_2Si particles. The primary Mg_2Si particles changed from coarse dendrites to regular polygons, and the average particle size decreased from 78.3 to 6.5 μm. Meanwhile, the Chinese eutectic Mg_2Si became small short fiber. The experimental results showed that the Nd_4Sb_3 phase could be formed after adding 1.0 wt.% Sb and 1.0 wt.% Nd to the alloy. The Nd_4Sb_3 phase could act as the heterogeneous nucleation core of Mg_2Si phase, which increased the nucleation rate of Mg_2Si and improved the morphology of Mg_2Si particles. The mechanical properties test found that the tensile properties and Brinell hardness of the alloy were improved with Sb and Nd alloyed. After adding 1.0 wt.% Sb and 1.0 wt.% Nd to the alloy, the ultimate tensile strength increased from 113 to 184 MPa, the elongation increased from 2.23 to 4.61%, and the Brinell hardness increased from 65.45 to 87.32 HB.

Keywords compound modification, magnesium alloy, mechanical property, Mg_2Si phase, microstructure

1. Introduction

Lightweight magnesium alloys have broad applications in various fields including electronic, aerospace (Ref 1, 2), and automation because of their high specific strength, high stiffness, relatively low density, good electrical conductivity, and excellent machinability (Ref 3, 4). However, one of the disadvantages of magnesium alloys is that the high-temperature mechanical properties of this material are somewhat poor, and this greatly limits broader industrial applications (Ref 5, 6).

Recent studies have reported methods to improve the heat-resistance problem of magnesium alloys such as microalloying (Ref 7), deformation strengthening (Ref 8), and second phase strengthening (Ref 9). Apparently, introducing Mg_2Si particles into the alloy was the most widely valuable because they are convenient and do not require complicated equipment. Furthermore, the Mg_2Si phase has some excellent characteristics such as low density (1.88 g/cm^3), high melting point (1087 °C), high hardness (HV 460), high elastic modulus (120 GPa), high elastic modulus (120 GPa),and low thermal expansion coefficient (7.5×10^{-6} K^{-1}) (Ref 10); the Mg_2Si phase can be stably present at high temperatures and enhance the mechanical properties of the material. Thus, the Mg_2Si phase is an ideal reinforcement phase for magnesium alloys.

However, many rough dendritic primary Mg_2Si and Chinese eutectic Mg_2Si are produced during the solidification of Mg-Si alloy throughout the magnesium matrix. These features negatively affect the physical properties of magnesium alloys. In view of this, optimizing the morphology and structure of Mg_2Si particles is necessary to improve the alloy performance.

There have been many studies demonstrating that the morphology of Mg_2Si can be modified upon adding different modifiers. Previous studies have indicated that coarse dendritic primary Mg_2Si particles were changed to regular polygons after adding Sb (Ref 11, 12), Nd (Ref 13, 14), Ba (Ref 15), or P (Ref 10, 16) to Mg-Si alloys: The modification mechanism of these elements can be concluded as the formation of a heterogeneous nucleation core of the Mg_2Si phase. In addition, the Y (Ref 17, 18), KBF_4 (Ref 19), and Bi (Ref 20) can also modify the coarse dendritic primary Mg_2Si because they inhibit the growth of Mg_2Si phase. Furthermore, the combination of two modifiers such as Ba-Sb (Ref 21), Sr-Sb (Ref 22), and Ca-Sb (Ref 23) can alert the coarse dendritic primary Mg_2Si as well. However, the size of most modification Mg_2Si particles is larger than 20 μm, and thus, we need more effective modifiers to further refine the primary Mg_2Si particles.

Previous studies have found that Sb transformed coarse dendritic primary Mg_2Si into regular polygonal particles by increasing the number of heterogeneous nucleation sites (Ref 11). Nd is also an effective modifier for Mg_2Si phase. Therefore, Sb and Nd would have synergistic modification effects. Thus, Nd and Sb were added to the Mg-4Si alloys to see the modification effect, and the objective of this work is to find an effective compound modifier and to evaluate the effect of Nd-Sb addition on the microstructure of Mg-4Si alloys, as well as to explore the mechanism of Nd and Sb compound modification.

Hao Dong, Siming Xiang, Jie Lv, Yu Wang, Lu Li, and **Wenbin Yu**, School of Materials and Energy, Southwest University, Chongqing 400715, China. Contact e-mails: 2994274741@qq.com, 2472271338@qq.com, lvjie.swu@foxmail.com, peientiandao1000@163.com, lilu.swu@gmail.com, and ywb2747@126.com.

2. Experimental Procedures

First, Mg ingot (> 99.9 wt.%) and Si ingot (> 99.8 wt.%) should be available for the preparation of Mg-4Si alloy. 1100 g pure Mg ingots were melted to 700 °C, and 40 g fine silicon particles were added to the metal solution after the pure magnesium is melted. And Mg ingot was added more due to Mg burned easily. A small amount of covering agent was added to the surface of the molten metal during the smelting process to protect the molten metal. This was held at 700 °C for 20 min and stirred evenly after slag removal. The molten magnesium solution can be poured into a cast iron mold preheated at 250 °C. This is the basis of subsequent experiments.

A previous study showed that the best modification effect was achieved after adding 1.0 wt.% Sb to the Mg-based alloy when adding a single modification element Sb (Ref 21). In this case, the only variable in the experiment was the difference in Nd content. The 1.0 wt.% Sb was added to the re-melted Mg-4Si alloys, and different amounts of Mg-30Nd alloy were added to the re-melted Mg-4Si alloys. The molten metal was kept at 700 °C for 20 min. After stirring, the molten metal was poured into a cast iron mold preheated at 250 °C to obtain the samples: This produced bars 20 mm in diameter. Table 1 shows the designed ratios of the Nd and Sb contents of the prepared ingots.

All metallographic samples in this experiment were taken from the same position of ingot. The samples were finely ground with different meshes of sandpaper, polished with a diamond spray polish, and then etched with 0.1% acetic acid. First of all, the phase constituent of the experimental Mg-4Si alloy was determined by XRD (Shimadzu XRD-7000) using Cu Kα radiation in step mode from 20° to 80° with a scanning speed of 2° min^{-1} and an acquisition step of 0.02°(2θ). After that, OLYMPUS-PMG3 optical microscope (OM) was used to observe the microstructure of the samples. Finally, AxioVision software was used to calculate the average size and density of Mg_2Si particles. The calculation process is as follows (Ref 24):

$$\text{Mean size} = \frac{1}{m}\sum_{j=1}^{m}\left(\frac{1}{n}\sum_{i=1}^{n}L_i\right)_j \quad \text{(Eq 1)}$$

$$\text{Mean density} = \frac{1}{m}\sum_{j=1}^{m}\left(\frac{1}{n}\sum_{i=1}^{n}D_i\right)_j \quad \text{(Eq 2)}$$

where L_i was the size of a single Mg_2Si particle and D_i is the density of Mg_2Si particles, respectively. Term n was the amount of Mg_2Si particles counted in this area at 71,300 μm^2, and m was the number of the measurement areas. A JSM-6610 scanning electron microscope (SEM) was used to analyze the microscopic appearance and element composition of the second phase. Nanoscale second phase particles were observed and analyzed by transmission electron microscopy (TEM), and the samples were prepared by focusing particle beams. Titan G2 60-300 model was used for TEM observation at 300 kV. The elemental composition of the second phase was obtained by mapping analysis, and the crystal structure of the second phase was determined by selected area electron diffraction.

Tensile test bars were prepared in accordance with the ASTMB557 M-02a standard, and the gauge length was set to 30 mm, and the cross section diameter was 6 mm. This tensile test was performed by use of a CMT5504 universal testing machine controlled by computer in the constant crosshead speed of 1 mm/min, and each sample was tested five times at room temperature. The fracture surface was observed by SEM, and the average ultimate tensile strength (UTS) and elongation were calculated. The hardness of samples was tested by use of a Brinell hardness tester (HBE-D3000A) under 2450 N load, with 15 s residence time and Φ 2.5 indenter. The present values in this paper are the average value of five random different positions.

Table 1 Alloy number and nominal Nd/Sb contents

Alloy number	1	2	3	4	5
Sb content, wt.%	0	1.0	1.0	1.0	1.0
Nd content, wt.%	0	0	0.5	1.0	2.0

3. Experiment Results and Discussion

3.1 Phase Analysis

Figure 1 shows the XRD examination results of Alloy 1 to 5, and it is clear that Mg_2Si phase and Mg phase were observed in the Mg-4Si alloy, indicating that Mg_2Si phase was formed during the solidification.

3.2 Microstructure Evolution

Figure 2 shows the microstructure of Mg-4Si alloys under different Nd and Sb addition values. The microstructure of unmodified Mg-4Si alloy (Fig. 2a) is composed of white α-Mg matrix, and Chinese eutectic Mg_2Si and coarse black primary Mg_2Si dendrites had a size of about 78 μm. According to the binary phase diagram of magnesium–silicon, dendritic primary Mg_2Si is first precipitated during the solidification process and then precipitates Chinese character eutectic Mg_2Si.

By adding 1.0 wt.% Sb to the Mg-4Si alloy, the morphology of primary Mg_2Si particles can significantly change from coarse dendrites to regular polygons (Fig. 2b) and the size reduced to about 20 μm, while the amount of Chinese eutectic Mg_2Si was

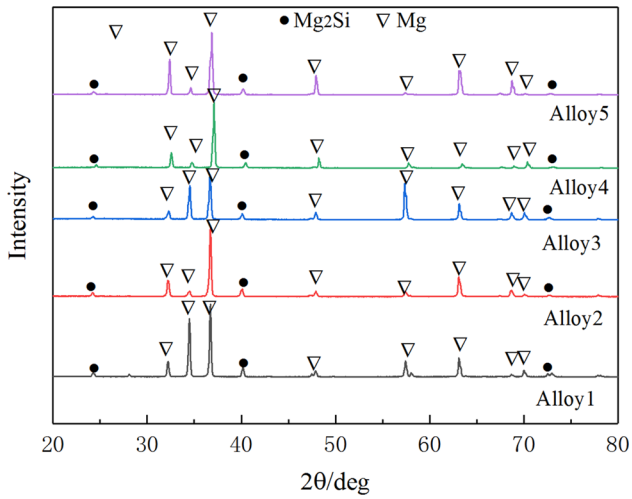

Fig. 1 XRD patterns of alloy 1, alloy 2, alloy 3, alloy 4, alloy 5

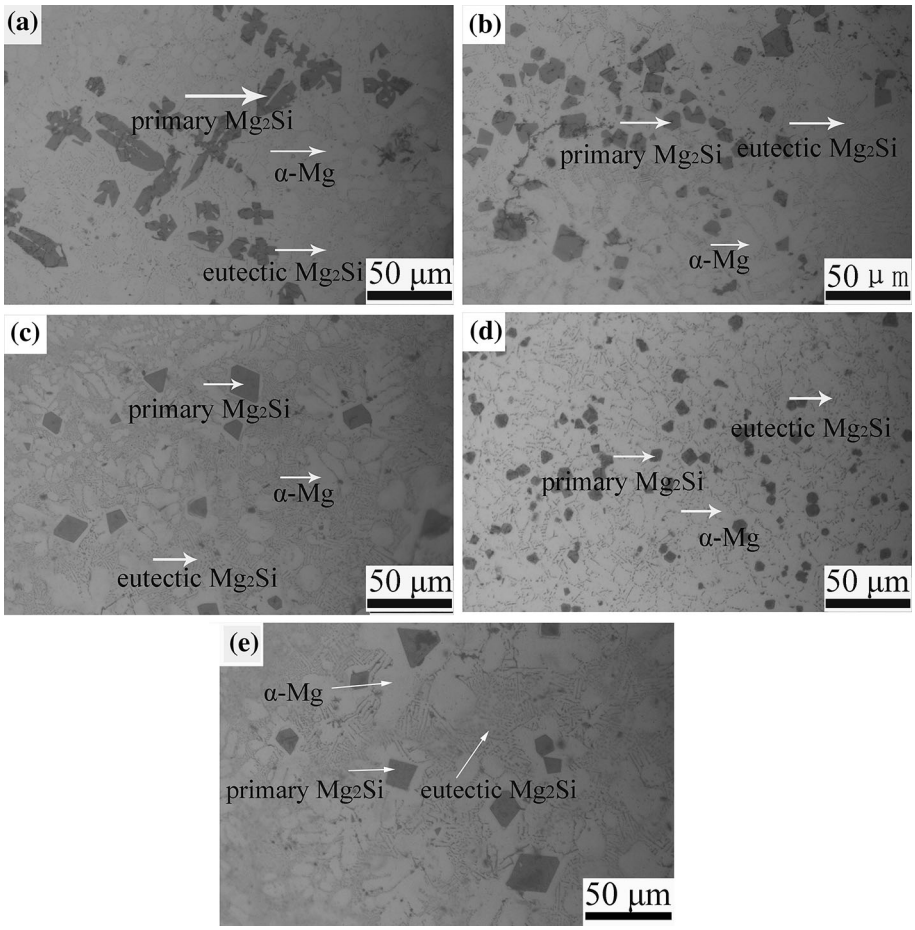

Fig. 2 Microstructures of Mg-4Si alloy (a) without modification and with modification of (b) 1.0 Sb, (c) 1.0 Sb-0.5 Nd, (d) 1.0 Sb-1.0 Nd, and (e) 1.0 Sb-2.0 Nd (wt.%)

reduced. To better modify the refined primary Mg_2Si particles, increasing ratios of Nd were added to the 1.0 wt.% Sb metamorphic Mg-4Si alloy. The addition of Nd makes the average particle size decrease significantly, and the particle size of primary Mg_2Si increases slightly when the addition amount of Nd is up to 1.0 wt.%.

Figure 2(c) shows that after adding 1.0 wt.% Sb and 0.5 wt.% Nd, the number of primary Mg_2Si particles decreased with increasing eutectic Mg_2Si content, and the particle size changed slightly. Figure 2(d) shows that with the increase in Nd content, the average size of primary Mg_2Si particles decreased significantly upon addition of 1.0 wt.% Nd. The Mg_2Si particles have the best polygon, and the average particle size obtained by OM is 6.5 μm. However, the amount of primary Mg_2Si particles decreased, and the size became larger when the Nd was continuously added to the alloy (Fig. 2e). At the same time, the changes in the average size and density of the primary Mg_2Si particles are plotted in Fig. 3; the density of the primary Mg_2Si particles increased with decreasing size. Figure 4 shows the magnified SEM observation on the alloys with different Sb and Nd addition, indicating that the Chinese-script eutectic Mg_2Si was significantly refined after the compound modification of Sb and Nd, and the amount of the eutectic Mg_2Si reduced with the addition of Nd up to 1.0 wt.%.

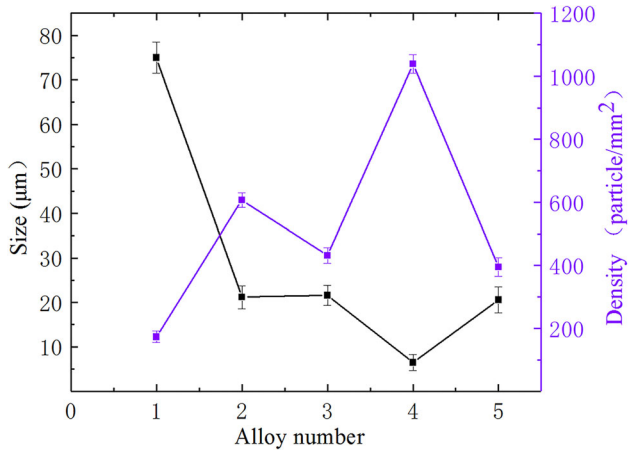

Fig. 3 Average size of primary Mg_2Si particles

3.3 Modification Mechanism

The results show that the addition of 1.0 wt.% Sb and 1.0 wt.% Nd has obvious compound modification effect on the primary Mg_2Si phase of Mg-4Si alloy. The modification mechanism of Nd and Sb on Mg-4Si alloy was studied by

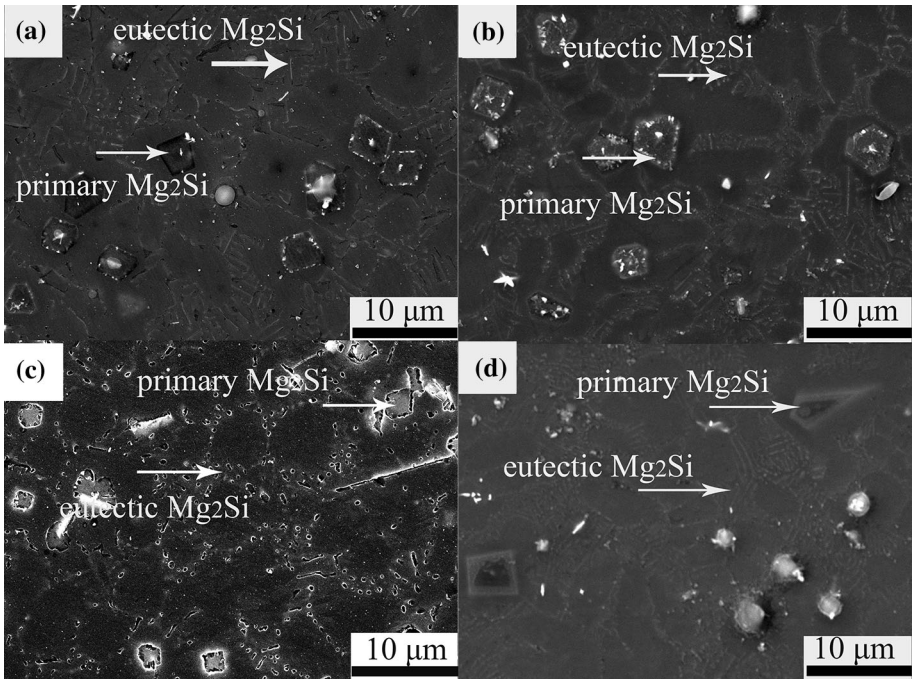

Fig. 4 Secondary electron SEM image of Mg-4Si alloy with chemical etched, (a) alloy 2, (b) alloy 3, (c) alloy 4, (d) alloy 5

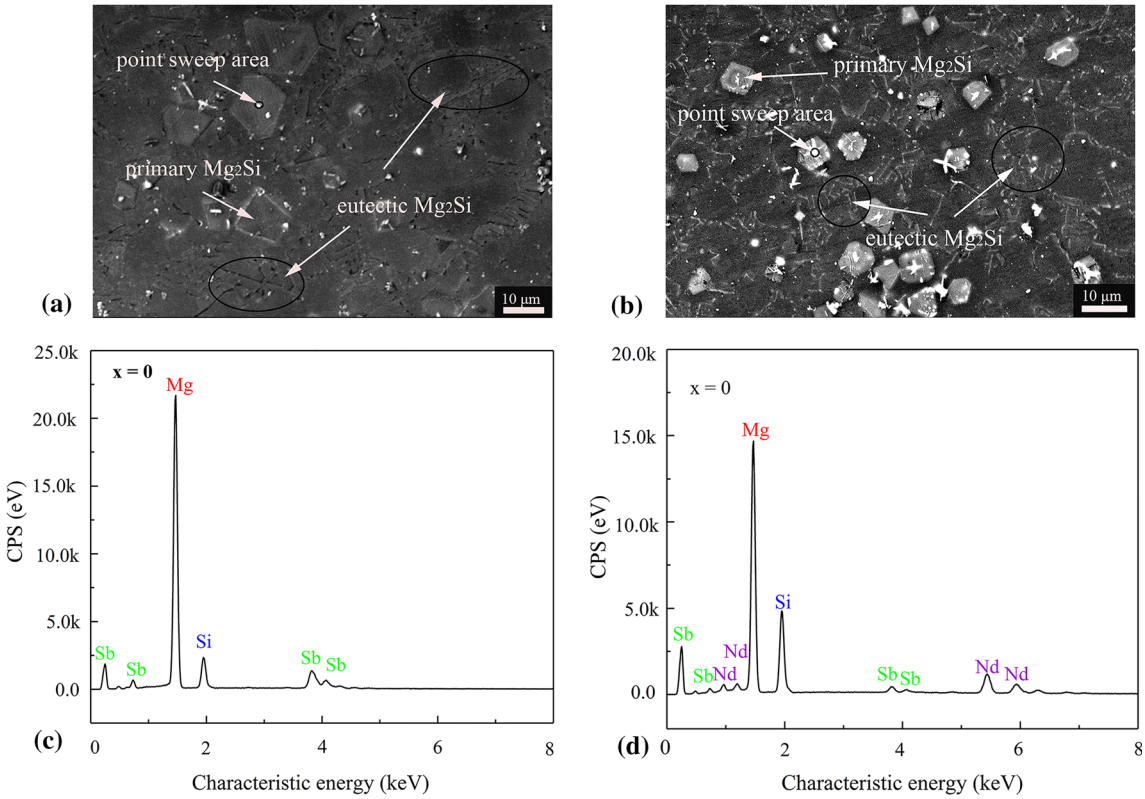

Fig. 5 (a) Secondary electron SEM image of Mg-4Si alloy with chemical etched modified with 1 wt.% Sb and (c) point EDS analysis; (b) SEM image of Mg-4Si alloy modified with 1.0 wt.% Sb and 1.0 wt.% Nd and (d) point EDS analysis

SEM. There were white cores in the middle or edge of the modified Mg_2Si phase (Fig. 5a and b), which could act as a heterogeneous nucleation core of the primary Mg_2Si particles. Figure 5(a) and (c) shows the SEM images and EDS analysis of the 1 wt.% Sb modified Mg-4Si alloy. Figure 5(a) shows that there are some white cores in the primary Mg_2Si particles. There is a point sweep of the white cores in Fig. 5(a), which reveals that the constituent elements of the white cores are Mg, Si, and Sb. Previous studies showed that the Mg_3Sb_2 phases can be formed in the Mg-Si alloy after adding Sb. These acted

as nucleation sites for the primary Mg_2Si particles (Ref 25). It can be seen from Fig. 5(a) that the Mg_3Sb_2 phase is too small, and the nucleation rate of the primary Mg_2Si was minimally improved, so the average size of the primary Mg_2Si particles was about 20 μm.

Figure 5(b) shows that the amount of white cores in the primary Mg_2Si particles obviously increased after adding 1 wt.% Sb and 1 wt.% Nd to the Mg-4Si alloy. Meanwhile, the average size of primary Mg_2Si particles decreased to 6.5 μm and was evenly distributed in the matrix; eutectic Mg_2Si changed from Chinese characters to small short fibers. The point sweep of the white core in the primary Mg_2Si particles in Fig. 5(d) reveals that there are Mg, Si, Sb, and Nd on the white cores—the possible intermetallic compounds between these elements include Mg_3Sb_2, $NdSi_2$, and Nd_4Sb_3.

The element composition of the core of the primary Mg_2Si particles will be confirmed in a future TEM study. Figure 6 shows a high-power bright TEM image with mapping analysis. The bright image (Fig. 6a) shows a dark phase that we think is the α-Mg phase, and there is also a white phase inside the Mg_2Si particles that is heterogeneous nucleation core of the primary Mg_2Si particles. The mapping analysis shows that there are Nd and Sb enrichments in the white core of the primary Mg_2Si particles (Fig. 6e and f). The white intermediate phase is likely a compound of Nd and Sb (Ref 26).

Figure 7 shows the high-power bright-field TEM image and selected area electron diffraction image of Mg-4Si alloy with 1.0 wt.% Sb and 1.0 wt.% alloyed Nd. The SAD pattern was collected from at least two regional axes by tilting the sample to determine the crystal structure (Ref 27). The target and selected area electron diffraction aperture were adjusted, and the intermetallics of Nd and Sb nanoparticles were studied. The area circled by the solid circle of 100 nm is the area of the selected area electron diffraction analysis. The SAD patterns were analyzed, and the results suggest that the core of the primary Mg_2Si consists of a Nd_4Sb_3 phase and a zone axis $A = [1\bar{3}1]$. Through these, the Nd_4Sb_3 phase has a cubic structure with lattice parameters of 0.9406 nm and belongs to

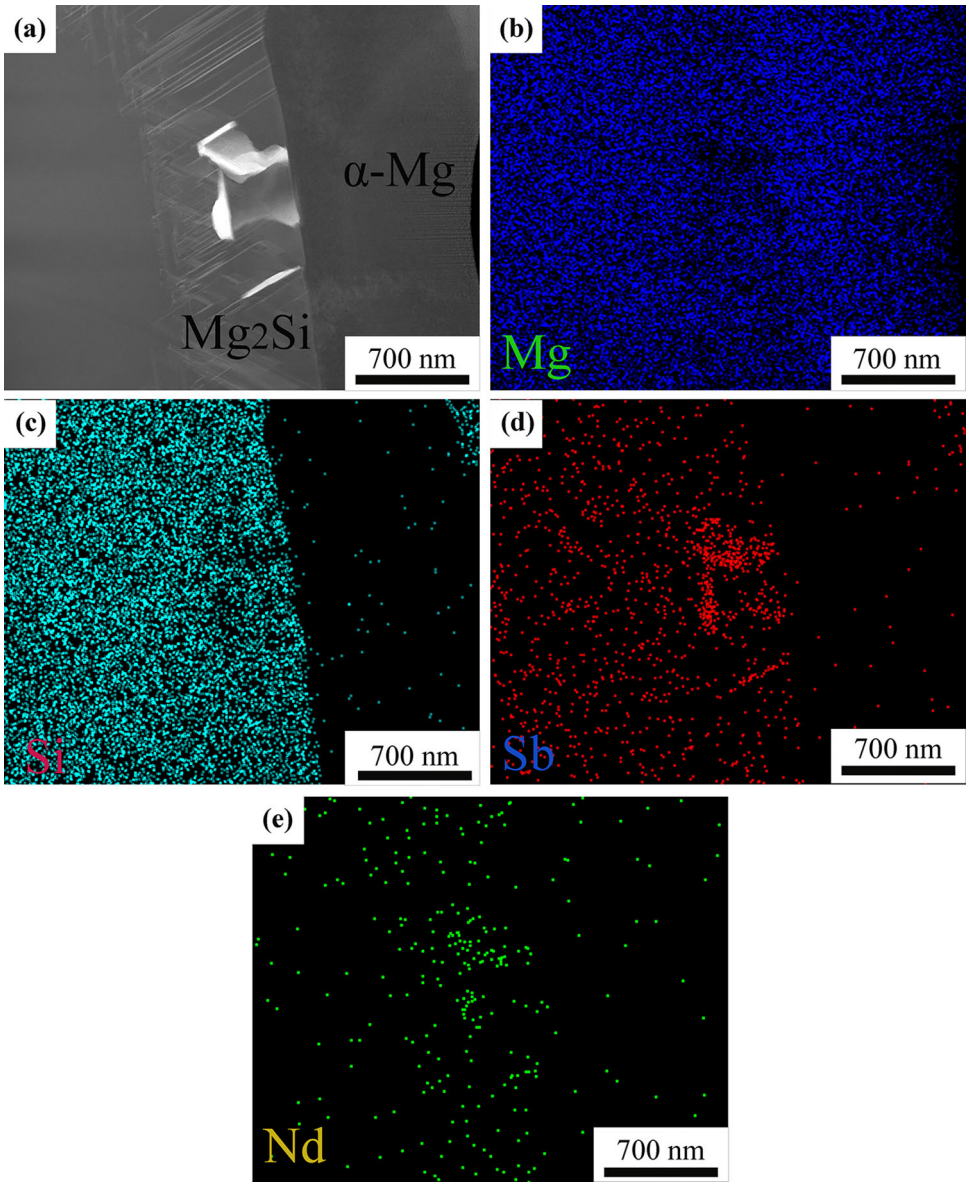

Fig. 6 (a) TEM bright image; EDS elemental mappings of (b) Mg; (c) Si; (d) Sb; and (e) Nd

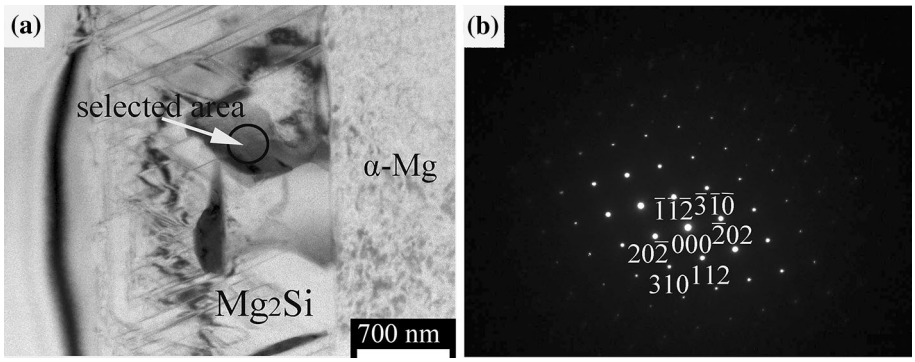

Fig. 7 (a) TEM bright image; (b) TEM SAD pattern taken from area circle

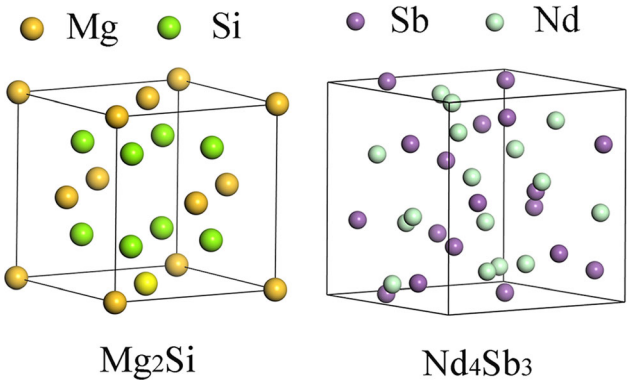

Fig. 8 Crystal structures of Mg_2Si and Nd_4Sb_3

the I-43d (220) space group. In addition, the Mg_2Si phase has a face-centered cubic structure with lattice parameters of 0.65 nm (Ref 28). This belongs to the Fm-3m (225) space group. Figure 8 shows the crystal structure of the Mg_2Si phase and the Nd_4Sb_3 phase, respectively.

In previous studies, the modification and refinement mechanism of different elements in Mg-4Si alloy was discussed. Adding alloying elements and appropriate modifiers can effectively change the morphology of Mg_2Si particles. This method is simple and efficient. The modification mechanism of the addition of Sb or Nd is to form a kind of heterogeneous nucleation core of Mg_2Si particles, and it will increase the nucleation rate (Ref 11, 14). For example, the Mg_3Sb_2 phase will be formed, while Sb was added to the Mg-Si alloys (Ref 12). These are the nucleation centers of primary Mg_2Si particles. When Nd is added to the alloy, $NdSi_2$ can play a similar role to the Mg_2Si particles (Ref 14). However, when Sb and Nd were added at the same time, no Mg_3Sb_2 or $NdSi_2$ particles were observed. In contrast, only Nd_4Sb_3 particles were detected in the newly formed phase; no other intermediate phase was observed. This can be explained by the differences in electronegativity of different atoms.

Electronegativity is a measure of an atom's ability to attract electrons. A higher electronegativity implies a stronger ability to attract electrons. In general, larger electronegativity differences lead to higher attraction and greater potential for compound formation. The electronegativity of Nd, Sb, Mg, and Si is 1.14, 2.05, 1.31, and 1.98, respectively. Obviously, the electronegativity difference between Nd and Sb is much larger than the electronegativity difference between Mg and Sb, or Nd and Si. Therefore, Nd and Sb combine to form Nd_4Sb_3 phases instead of Mg_3Sb_2 phases and $NdSi_2$ phases as other studies have done.

In order to investigate whether the Nd_4Sb_3 phase can be used as the heterogeneous nucleation core of the Mg_2Si phase, the lattice mismatch between Nd_4Sb_3 and Mg_2Si was calculated according to Bramfitt theory. The Bramfitt theoretical calculation formula is shown as follows (Ref 25):

$$\delta_{(hkl)n}^{(hkl)s} = \frac{1}{3}\sum_{i=1}^{3}\frac{\left|d[uvw]_s^i\cos\theta - d[uvw]_n^i\right|}{3d_{[uvw]_n}^i} \quad \text{(Eq 3)}$$

Here, $(hkl)_s$ is the low-index crystal plane of the heterogeneous substrate, and $[uvw]_s$ is the low-index crystal orientation in the $(hkl)_s$ plane. Term $(hkl)_n$ is the low-index crystal plane of the new crystal nucleus, and $[uvw]_n$ is the low-index crystal orientation in the $(hkl)_n$ plane. Terms $d_{[uvw]s}$ and $d_{[uvw]n}$ are atomic spatial distances along the $[uvw]_s$ and $[uvw]_n$ orientations, and θ is the angle between $[uvw]_s$ and $[uvw]_n$ orientations ($\theta < 90°$).

Through the study of Bramfitt theory, the energy at the boundary of the heterogeneous nucleation core and the Mg_2Si phase affects the formation of the heterogeneous core. This is mainly related to the energy at the contact surface, and the key to the formation of the heterogeneous nucleation core is that the lattice mismatch of the contact surface is less than 15%.

Figure 9 shows the (001) crystal plane of the Mg_2Si phase and the (211) crystal plane of the Nd_4Sb_3 phase. The planar mismatch of some possible crystallographic orientations for Mg_2Si nucleation on the Nd_4Sb_3 particles was calculated according to Fig. 9 and Bramfitt theory. Table 2 shows that the disregistry reaches 9.33% when the orientation relationship between Nd_4Sb_3 and Mg_2Si is $(211)_{Nd4Sb3}\|(001)_{Mg2Si}$. From Bramfitt's theory, the mismatch between two-phase planes is less than 15%, and one phase can act as a heterogeneous nucleation point for the other phase. Therefore, the Nd_4Sb_3 phase can be used as a heterogeneous nucleus of primary Mg_2Si phase. The formation of a large number of fine Nd_4Sb_3 particles improved the nucleation rate of primary Mg_2Si particles. Therefore, during solidification, the core of the primary Mg_2Si increases and is evenly distributed in the matrix. The primary Mg_2Si particles do not grow into dendritic crystals, but rather become a small regular polygon.

The results show that the average size of the primary Mg_2Si particles is much smaller than that of the single Nd or Sb element after adding Nd and Sb at the same time. This is due to that adding 1.0 wt.% Nd and 1.0 wt.% Sb to Mg-4Si alloy can form a Nd_4Sb_3 phase, which is the heterogeneous nucleation

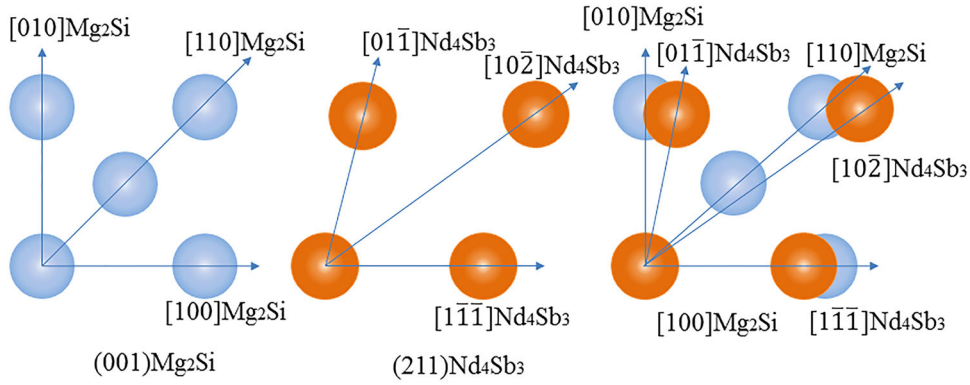

Fig. 9 Comparison of atomic arrangements in (001) Mg_2Si and (211) Nd_4Sb_3

Table 2 Calculated values for planar disregistry between Mg_2Si and Nd_4Sb_3

	(001)Nd_4Sb_3‖(001) Mg_2Si			**(110)Nd_4Sb‖(001) Mg_2Si**			**(211)Nd_4Sb_3‖(001) Mg_2Si**		
(*hkl*)Nd_4Sb_3	[010]	[320]	[120]	[$\bar{1}$00]	[$\bar{2}$10]	[$\bar{3}$20]	[1$\bar{1}\bar{1}$]	[10$\bar{2}$]	[01$\bar{1}$]
(*hkl*)Mg_2Si	[100]	[110]	[010]	[100]	[110]	[010]	[100]	[110]	[010]
d(*hkl*)Nd_4Sb_3	9.40	2.59	4.19	9.40	4.19	2.59	5.41	6.35	6.42
d(*hkl*)Mg_2Si	6.35	4.49	6.35	6.35	4.49	6.35	6.35	4.49	6.35
θ deg	0	12	0	0	15	0	0	15	10
δ		46.15			40.23			9.33	

center of primary Mg_2Si particles. Therefore, the nucleation rate of the primary Mg_2Si phase is greatly increased, and the morphology of Mg_2Si changes from a coarse dendritic shape to a regular polygon. However, as the Nd content exceeds 1.0 wt.%, the primary Mg_2Si particles begin to grow slightly larger. This is because of the Nd-Sb binary phase diagram. The Nd_4Sb_3 phase can be formed when the contents of Nd and Sb are close to each other. With increasing addition of Nd, the Nd_5Sb_3 phase can finally be formed, but it cannot act as a heterogeneous nucleation site for the primary Mg_2Si particles. Therefore, the nucleation rate of primary Mg_2Si decreases and the primary Mg_2Si particles become much larger. Meanwhile, the amount of Chinese eutectic Mg_2Si increases sharply with much more alloyed Nd. This is called the over-modification phenomenon.

3.4 Mechanical Properties

The tensile mechanical properties and hardness of different samples were tested to investigate the effect of adding different amounts of modifier on the mechanical properties of Mg-4Si alloy (Fig. 10 and 11).

3.4.1 Hardness. The change of hardness can be found in Fig. 10 of Mg-4Si alloy after adding different amounts of Nd and Sb. Figure 10 shows that the Brinell hardness of the unmodified Mg-4Si alloy is at least HB 65.45, and the Brinell hardness value of the alloy first increases and then decreases upon addition of different amounts of modifiers. The maximum value was HB 89.17, and this was achieved upon modification of 1.0 wt.% Sb and 1.0 wt.% Nd. These results indicate that the hardness value of the Mg-4Si alloy is related to the morphology of the primary Mg_2Si particles. The fine regular polygonal

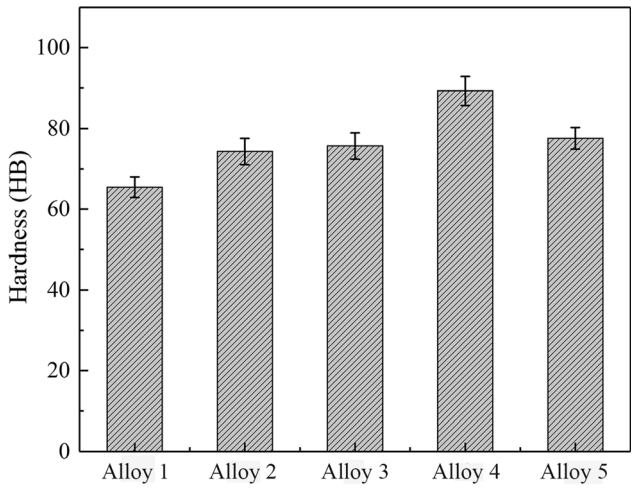

Fig. 10 Effect of different contents of Sb and Nd on the Brinell hardness of Mg-4Si alloy

particles contribute to the improvement of the hardness. This is because the stress at the contact point of the Mg_2Si particles with the magnesium matrix is reduced after deformation. Thus, it is difficult to initiate cracks at the interface between the primary Mg_2Si particles and magnesium matrix. Thus, the hardness of the alloy increased via 1.0 wt.% Sb and 1.0 wt.% Nd modification.

3.4.2 Tensile Properties and Fracture Characteristics. Tensile properties of Mg-4Si alloy modified by different content Sb and Nd are shown in Fig. 11. The ultimate tensile strength in the experiment is raised from 113.24 to 175.38 MPa

when the Mg-4Si alloy was modified by adding 1.0 wt.% Nd and 1.0 wt.% Sb. With the elongation increases from 2.23% to 4.61%, it is clear that improvement of the mechanical properties of the alloy is closely related to the morphology of the Mg_2Si-reinforced phase. This is because of the thermal expansion coefficient between the matrix and the reinforcing phase and the Griffith formula.

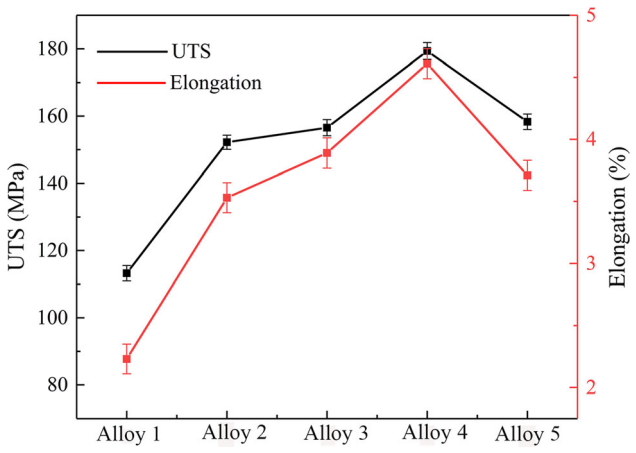

Fig. 11 Effect of different contents of Sb and Nd on the tensile properties of Mg-4Si alloy

An improved coefficient of thermal expansion (CTE) mismatch can increase the ultimate tensile strength of the Mg-4Si alloy (Ref 29). Due to the large difference in the CTE between α-Mg and Mg_2Si reinforcement phase, there is a relatively large residual stress between Mg_2Si and magnesium matrix during alloy smelting. Residual stress concentration at the grain boundary produces many high-density dislocations between the magnesium matrix and the Mg_2Si reinforcing phase, and the dislocation motion of the material becomes more difficult resulting in an increase in the strength of the material. The CTE mismatch is related to the size and shape of the reinforcing phase particles(Ref 30). The eutectic Mg_2Si was still refined after adding 1.0 wt.% Sb and 1.0 wt.% Nd to the Mg-4Si alloy; thus, the alloys were further strengthened with the addition of Nd up to 1.0 wt.%.

The other strengthening mechanism is related to the size of the primary Mg_2Si particles; the relationship between the particle diameter (d) and the fracture stress (σ_c) was demonstrated by the Griffith equation as follows (Ref 12):

$$\sigma_c = k_c d^{-0.5} \quad \text{(Eq 4)}$$

Here, k_c is the fracture toughness of the particle, and d is the diameter of the particle. Griffith's theory states that the fracture stress of the test alloy increases with decreased particle diameter. The primary Mg_2Si particle size decreases signifi-

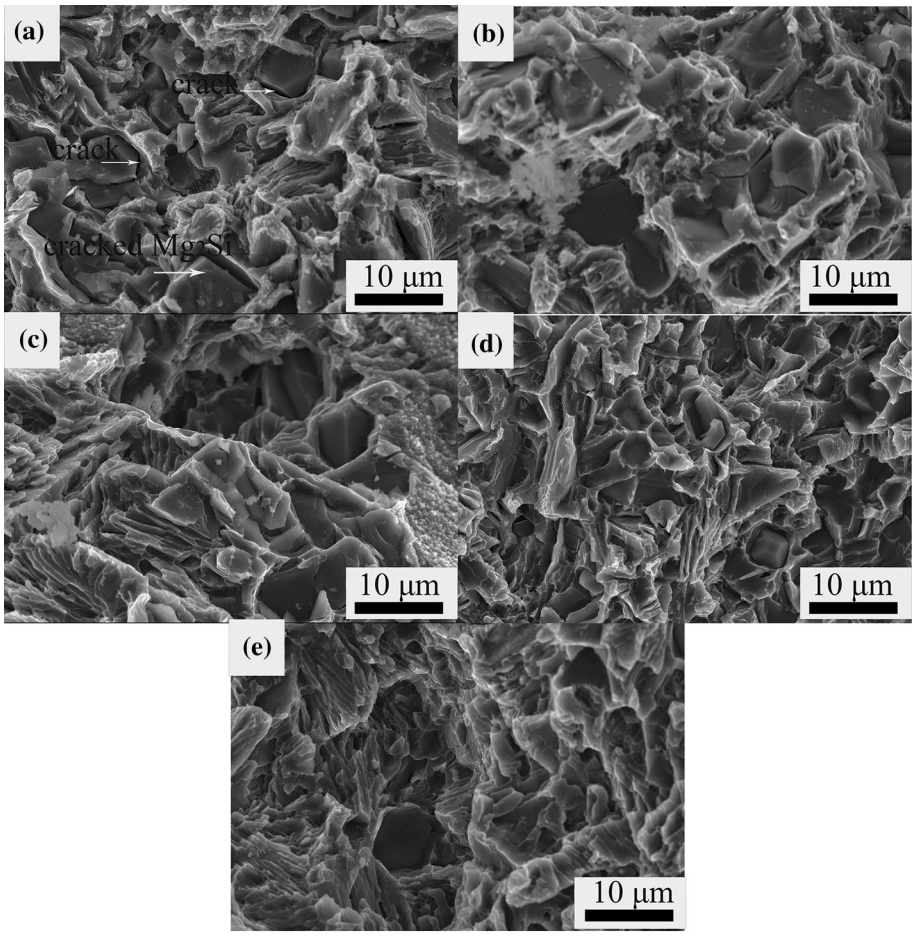

Fig. 12 Representative micrograph of a fractured surface on the Mg-4Si alloy: (a) alloy 1; (b) alloy 2; (c) alloy 3; (d) alloy 4; (e) alloy 5

cantly in the Mg-4Si alloy with the addition of 1.0 wt.% Nd and 1.0 wt.% Sb. This means that more stress is needed to break the Mg-4Si alloy after 1.0% Nd and 1.0% Sb addition. This improves the UTS and elongation values.

The typical fracture surface of the test alloy after adding different amounts of Nd and Sb to the alloys is shown in Fig. 12. Figure 12(a) shows that the cross section of the unmodified Mg-4Si alloy consists of a flat tearing surface on the Mg_2Si particles. These tearing surfaces are irregularly shaped with cracks. This is attributed to the presence of coarse dendritic primary Mg_2Si and Chinese eutectic Mg_2Si in the unmodified Mg-4Si alloy. The sharp edges of the unmodified primary Mg_2Si particles generate a large amount of stress when they are in contact with the magnesium matrix, and these particles are concentrated at the grain boundaries. The crack is generated under a tensile load, and this crack expanded along the edge of the unmodified primary Mg_2Si and eutectic Mg_2Si, which will reduce the strength and elongation of the alloy.

Figure 12(b–e) shows the fracture surface of the alloy with different Nd and Sb addition. It can be seen that the smaller the particles falling off, the less obvious the crack growth is. The Mg_2Si phase prefers to act as the potential crack initiation site, so the refined Mg_2Si phases could decrease the stress concentration and prevent the crack initiation (Ref 31, 32). This indicated that the ultimate tensile strength improved due to that the morphology of primary Mg_2Si was changed from coarse dendrite to regular polygon by the addition of Sb and Nd. Meanwhile, the morphology of eutectic Mg_2Si was changed from Chinese character to small short rod. Small fine polygonal Mg_2Si particles are benefitted to prevent the generation and development of cracks. Therefore, the ultimate tensile strength and elongation of the alloy have been greatly improved.

4. Conclusions

(1) The effect of the addition of Sb and Nd compound modification is as follows: The morphology of primary Mg_2Si particles changes from coarse dendrite to regular shaped polygon, and the average size of the primary Mg_2Si particles decreased to 6.5 μm from 78 μm after adding 1.0 wt.% of Sb and 1.0 wt.% Nd. Furthermore, the amount of eutectic Mg_2Si reduced with addition of Nd elements up to 1.0 wt.%. The Chinese-shaped eutectic Mg_2Si is metamorphosed into a small short rod shape distributed in matrix. Therefore, the simultaneous addition of Sb and Nd is much better than the addition of Sb or Nd alone.

(2) The Nd_4Sb_3 phase appeared in the core of the primary Mg_2Si particles after adding 1 wt.% Nd and 1 wt.% Sb to the Mg-4Si alloy. The crystal lattice mismatch between Nd_4Sb_3 and Mg_2Si was 9.33% (less than 15%), and thus, the Nd_4Sb_3 phase can be used as heterogeneous nucleation core of primary Mg_2Si particles. Therefore, the nucleation rate of the Mg_2Si phase is increased, and the primary Mg_2Si particles become regular and uniformly distributed in the magnesium matrix.

(3) The hardness and tensile strength of the alloy increased with the modification of Sb and Nd. The Brinell hardness of the alloy increased from HB 65.45 to HB 89.17. In addition, the mechanical properties showed that the UTS value increased from 113.24 to 175.38 MPa, and the elongation changes from 2.23 to 4.61%. These are attributed to the compound modification for primary and eutectic Mg_2Si particles.

Acknowledgments

We thank LetPub (www.letpub.com) for linguistic assistance during the preparation of this manuscript. This work was supported by the National Natural Science Foundation of China (Grant numbers 51975484 and 51605392).

Funding

This study was funded by 51975484 and 51605392.

Conflict of interest

The authors declare that they have no conflict of interest.

References

1. W. Jiang, G. Li, Z. Fan, L. Wang, and F. Liu, Investigation on the Interface Characteristics of Al/Mg Bimetallic Castings Processed by Lost Foam Casting, *Metall. Mater. Trans. A*, 2016, **47**, p 2462–2470
2. Z. Jiang, Z. Fan, W. Jiang, G. Li, Y. Wu, F. Guan et al., Interfacial Microstructures and Mechanical Properties of Mg/Al Bimetal Produced by a Novel Liquid–Liquid Compound Casting Process, *J. Mater. Process. Technol.*, 2018, **261**, p 149–158
3. H.R. Bakhsheshi-Rad, E. Hamzah, S. Farahany, and M.P. Staiger, The Mechanical Properties and Corrosion Behavior of Quaternary Mg-6Zn-0.8Mn-xCa Alloys, *J. Mater. Eng. Perform.*, 2014, **24**, p 598–608
4. Y. Chen, L. Wang, Y. Feng, E. Guo, S. Zhao, and L. Wang, Effect of Ca and Sm Combined Addition on the Microstructure and Elevated-Temperature Mechanical Properties of Mg-6Al Alloys, *J. Mater. Eng. Perform.*, 2019, **28**, p 2892–2902
5. M. Cong, Z. Li, J. Liu, M. Yan, K. Chen, Y. Sun et al., Effect of Ca on the Microstructure and Tensile Properties of Mg–Zn–Si Alloys at Ambient and Elevated Temperature, *J. Alloys Compd.*, 2012, **539**, p 168–173
6. W. Jiang, Z. Fan, G. Li, L. Yang, and X. Liu, Effects of Melt-to-Solid Insert Volume Ratio on the Microstructures and Mechanical Properties of Al/Mg Bimetallic Castings Produced by Lost Foam Casting, *Metall. Mater. Trans. A*, 2016, **47**, p 6487–6497
7. X. Qian, N. Parson, and X.G. Chen, Effect of Homogenization Treatment and Microalloying with Mn on the Microstructure and Hot Workability of AA6060 Aluminum Alloys, *J. Mater. Eng. Perform.*, 2019, **28**, p 4531–4542
8. T. Sakthivel, G. Sasikala, M.K. Dash, and P. Syamala Rao, Creep Deformation and Rupture Behavior of P92 Steel Weld Joint Fabricated

by NG-TIG Welding Process, *J. Mater. Eng. Perform.*, 2019, **28**, p 4364–4378
9. P. Nieroda, A. Kolezynski, J. Leszczynski, J. Nieroda, and P. Pasierb, The Structural, Microstructural and Thermoelectric Properties of Mg_2Si Synthesized by SPS Method Under Excess Mg Content Conditions, *J. Alloys Compd.*, 2019, **775**, p 138–149
10. C. Li, X. Liu, and Y. Wu, Refinement and Modification Performance of Al–P Master Alloy on Primary Mg_2Si in Al–Mg–Si Alloys, *J. Alloys Compd.*, 2008, **465**, p 145–150
11. L. Liao, X. Zhang, H. Wang, X. Li, and N. Ma, Influence of Sb on Damping Capacity and Mechanical Properties of Mg_2Si/Mg–9Al Composite Materials, *J. Alloys Compd.*, 2007, **430**, p 292–296
12. H.Y. Wang, F. Liu, L. Chen, M. Zha, G.J. Liu, and Q.C. Jiang, The Effect of Sb Addition on Microstructures and Tensile Properties of Extruded Al–20Mg_2Si–4Cu Alloy, *Mater. Sci. Eng. A*, 2016, **657**, p 331–338
13. K.K.A. Kumar, A. Viswanath, U.T.S. Pillai, B.C. Pai, and M. Chakraborty, Influence of Neodymium Addition on the Microstructure, Mechanical and Thermal Properties of Mg-Si Alloys, *Proc. Eng.*, 2013, **55**, p 103–108
14. H. J-l, C.-p. Tang, X.-m. Zhang, and Y.-l. Deng, Modification of Mg_2Si in Mg-Si Alloys with Neodymium, *Trans. Nonferr. Met. Soc.*, 2013, **23**, p 3161–3166
15. K. Chen, Z.Q. Li, J.S. Liu, J.N. Yang, Y.D. Sun, and S.G. Bian, The Effect of Ba Addition on Microstructure of in Situ Synthesized Mg_2Si/Mg–Zn–Si Composites, *J. Alloys Compd.*, 2009, **487**, p 293–297
16. J. Hou, C. Li, and X. Liu, Nucleating Role of an Effective in Situ Mg_3P_2 on Mg_2Si in Mg–Al–Si Alloys, *J. Alloys Compd.*, 2011, **509**, p 735–739
17. Q.C. Jiang, H.Y. Wang, Y. Wang, B.X. Ma, and J.G. Wang, Modification of Mg_2Si in Mg–Si Alloys with Yttrium, *Mater. Sci. Eng. A*, 2005, **392**, p 130–135
18. G. Mao, H. Yan, C. Zhu, Z. Wu, and W. Gao, The Varied Mechanisms of Yttrium (Y) Modifying a Hypoeutectic Al–Si Alloy Under Conditions of Different Cooling Rates, *J. Alloys Compd.*, 2019, **806**, p 909–916
19. M.-B. Yang, F.-S. Pan, J. Shen, and L. Bai, Comparison of Sb and Sr on Modification and Refinement of Mg_2Si Phase in AZ61-0.7Si Magnesium Alloy, *Trans. Nonferr. Met. Soc.*, 2009, **19**, p 287–292
20. X.-F. Wu, Y. Wang, K.-Y. Wang, R.-D. Zhao, and F.-F. Wu, Enhanced Mechanical Properties of Hypoeutectic Al-10Mg_2Si Cast Alloys by Bi Addition, *J. Alloys Compd.*, 2018, **767**, p 163–172
21. K. Chen and Z. Li, Effect of Co-modification by Ba and Sb on the Microstructure of Mg_2Si/Mg–Zn–Si Composite and Mechanism, *J. Alloys Compd.*, 2014, **592**, p 196–201
22. D.H. Kang, G.T. Bae, and N.J. Kim, Effect of Sb and Sr Additions on the Microstructural Evolution of Mg-Sn-Al-Si Based Alloys, *Mater. Trans.*, 2008, **49**, p 936–940
23. H.-C. Yu, H.-Y. Wang, L. Chen, M. Zha, C. Wang, C. Li et al., Spheroidization of Primary Mg_2Si in Al-20Mg_2Si-4.5Cu Alloy Modified with Ca and Sb During T6 Heat Treatment Process, *Mater. Sci. Eng. A*, 2017, **685**, p 31–38
24. S. Farahany, H. Ghandvar, N.A. Nordin, A. Ourdjini, and M.H. Idris, Effect of Primary and Eutectic Mg_2Si Crystal Modifications on the Mechanical Properties and Sliding Wear Behaviour of an Al–20Mg_2Si–2Cu–xBi Composite, *J. Mater. Sci. Technol.*, 2016, **32**, p 1083–1097
25. Y. Wang and X. Guo, Heterogeneous Nucleation of Mg_2Si and $Mg_2(Si, Sn)$ on Mg_3Sb_2 Nucleus in Mg Containing Si Alloys, *Mater. Chem. Phys.*, 2019, **223**, p 336–342
26. L. Sheng, L. Wang, T. Xi, Y. Zheng, and H. Ye, Microstructure, Precipitates and Compressive Properties of Various Holmium Doped NiAl/Cr(Mo, Hf) Eutectic Alloys, *Mater. Des.*, 2011, **32**, p 4810–4817
27. H. Chang Shin, J. Son, B.K. Min, Y.S. Choi, K.M. Cho, D.H. Cho et al., The Effect of Ce on the Modification of Mg_2Si Phases of As-Cast Eutectic Mg-Si Alloys, *J. Alloys Compd.*, 2019, **792**, p 59–68
28. A. Gil-Santos, I. Marco, N. Moelans, N. Hort, and O. Van der Biest, Microstructure and Degradation Performance of Biodegradable Mg-Si-Sr Implant Alloys, *Mater. Sci. Eng. C Mater. Biol. Appl.*, 2017, **71**, p 25–34
29. M. Wang, D. Chen, Z. Chen, Y. Wu, F. Wang, N. Ma et al., Mechanical Properties of in Situ TiB_2/A356 Composites, *Mater. Sci. Eng. A*, 2014, **590**, p 246–254
30. R. Du, D. Yuan, F. Li, D. Zhang, S. Wu, and S. Lü, Effect of in Situ TiB_2 Particles on Microstructure and Mechanical Properties of Mg_2Si/Al Composites, *J. Alloys Compd.*, 2019, **776**, p 536–542
31. B.N. Du, Z.P. Xiao, Y.X. Qiao, L. Zheng, B.Y. Yu, D.K. Xu et al., Optimization of Microstructure and Mechanical Property of a Mg-Zn-Y-Nd Alloy by Extrusion Process, *J. Alloys Compd.*, 2019, **775**, p 990–1001
32. L.-Y. Sheng, F. Yang, T.-F. Xi, Y.-F. Zheng, and J.-T. Guo, Microstructure and Room Temperature Mechanical Properties of NiAl–Cr(Mo)–(Hf, Dy) Hypoeutectic Alloy Prepared by Injection Casting, *Trans. Nonferr. Met. Soc.*, 2013, **23**, p 983–990